Enhancing Seismic Resilience of Electric Power Distribution Systems with Mobile Power Sources

Zijiang Yang, *Student Member, IEEE,* Payman Dehghanian, *Member, IEEE*, and Mostafa Nazemi, *Student Member, IEEE*

***Abstract*—Mobile power sources (MPSs), including mobile emergency generators (MEGs), truck-mounted mobile energy storage systems (MESSs) and electric vehicles (EVs) have great potentials to be employed as grid-support resources during power grid emergency operating conditions to supply the critical loads and enhance the resilience of distribution system (DS) via a swift disaster restoration. We here investigate the MPS dispatch (i.e., routing and scheduling) in coordination with DS dynamic network reconfiguration. We propose a two-stage restoration scheme to facilitate the DS restoration following the high-impact low-probability (HILP) seismic disasters. In the first stage, a seismic hazard is simulated through a Monte-Carlo simulation (MCS) engine to estimate the unavailability of power distribution branches under a suite of seismic force scenarios. In the second stage, a mixed-integer nonlinear programming (MINLP) optimization model is formulated for DS restoration that co-optimizes the routing and scheduling of MPSs and DS dynamic network reconfiguration. The MINLP model is then linearized to a mixed-integer linear programming (MILP) model to reduce the computation complexity, where the seismic-resilience recovery strategies are generated at different timescales. The efficacy of the proposed method is evaluated on the IEEE 33-node test system and the results verify a significant reduction in the load outages and an improved power system resilience to HILP earthquakes.**

***Index Terms*—Distribution systems (DS); high-impact low-probability (HILP) hazards; mobile power sources (MPS); routing and scheduling; seismic resilience; dynamic reconfiguration.**

NOMENCLATURE

A. Sets and Indices

$i, j \in \mathbf{B}$	Indices/set of nodes.
$m \in \mathbf{M}$	Indices/set of mobile power sources (MPSs).
$t, \tau \in \mathbf{T}$	Indices/set of time periods.
$(i, j) \in \mathbf{L}$	Indices/set of branches.
$N_{\mathbf{B}}, N_{\mathbf{T}}, N_{\mathbf{L}}$	Number of all nodes, time periods, branches.
$\mathbf{B}^{\text{sub}}$	Set of substation nodes.
$\mathbf{B}_m$	Set of candidate nodes that can be connected to MPS m.
$\mathbf{B}_t^{\text{source}}$	Set of nodes that are selected to be the sources of the fictitious flows at time t.
$\mathbf{L}^{\text{switch}}$	set of branches equipped with remotely-controlled switches.
$\mathbf{L}_t^{\text{damaged}}$	Set of branches that are damaged and have not been repaired at time t.
$\mathbf{G} \in \mathbf{M}$	Set of all mobile emergency generators (MEGs).
$\mathbf{S} \in \mathbf{M}$	Set of all mobile energy storage systems (MESSs).
$\mathbf{V} \in \mathbf{M}$	Set of all mobile electric vehicle (EV) fleets.
$\mathbf{M_i}$	Set of MPSs that can be connected to node i.

B. Parameters and Constants

χ_i	Priority of the load demanded at node i.
$\beta_{ij,t}$	Binary damage status of the branch (i, j) at time t (1 if the branch is undamaged or has been repaired, 0 otherwise).
$P_{i,t}^{\text{demand}}$	Real power demand of node i at time t (kW).
$Q_{i,t}^{\text{demand}}$	Reactive power demand of node i at time t (kVar).
α_{ij}^0	Binary parameter representing the initial status of branch (i,j) (1 if the branch is connected, 0 otherwise).
N_t^{island}	Number of islands due to the damaged and unrepaired branches at time t.
N_i^{mps}	Number of MPSs that are allowed to be connected to node i.
$T_{m,ij}^{\text{travel}}$	Travel time of MPS m from node i to node j.
Δt	Duration of one time period.
M	A large enough positive number.
$\underline{\text{SOC}}_m$	Minimum state of charge (SOC) of MESS or EV fleet m (kWh).
$\overline{\text{SOC}}_m$	Maximum SOC of the MESS or EV fleet m (kWh).
$\overline{P}_m^{\text{ch}}, \overline{P}_m^{\text{dch}}$	Maximum charging and discharging power of MESS or EV fleet m (kW, kVar).
$\overline{P}_m, \overline{Q}_m$	Maximum real and reactive power output of MPS m (kW, kVar).
$\overline{P}_{ij}, \overline{Q}_{ij}$	Real and reactive power capacity of branch (i, j) (kW, kVar).
r_{ij}, x_{ij}	Resistance and reactance of branch (i, j) (Ω).
$\underline{\text{Vsqr}}_i$	Minimum squared voltage magnitude at node i (kV^2).
$\overline{\text{Vsqr}}_i$	Maximum squared voltage magnitude at node i (kV^2).
C_m^{tr}	Transportation cost coefficient of MPS m.
C_m^{P}	Power rating price of MESS or EV fleet m (\$/kWh).

Z.Yang, P. Dehghanian, and M. Nazemi are with the Department of Electrical and Computer Engineering, George Washington University, Washington, DC 20052, USA (e-mails: zyang55@gwu.edu; payman@gwu.edu; mostafa_nazemi@gwu.edu).

978-1-5386-4539-0/19/$31.00 © 2019 IEEE

k_m Degradation slope of MESS or EV feelt m.

δ_m Generation cost coefficient of MEG m.

$\eta_m^{\text{ch}}, \eta_m^{\text{dch}}$ Charging and discharging efficiency of MESS or EV fleet m.

P_m^{travel} Energy Consumption rate of EV fleet m when traveling (kW).

$d_{i,t}^{\text{fic}}$ Fictitious load of node i at time t.

C. Functions and Variables

$pd_{i,t}, qd_{i,t}$ Real and reactive power demand supplied at node i at time t (kW, kVar).

$pg_{i,t}, qg_{i,t}$ Real and reactive power at substation node i at time t (kW, kVar).

$pf_{ij,t}, qf_{ij,t}$ Real and reactive power flow on branch (i, j) at time t (kW, kVar).

$\text{SOC}_{m,t}$ SOC of MESS or EV fleet m at time t (kWh).

$p_{m,t}^{\text{ch}}, p_{m,t}^{\text{dch}}$ Charging and discharging power of MESS or EV fleet m at time t (kW).

$p_{m,t}, q_{m,t}$ Real and reactive power output of MPS m at time t (kW, kVar).

$p_{i,t}^{\text{mps}}, q_{i,t}^{\text{mps}}$ Real and reactive power output of MPS at node i (kW, kVar).

$Vsqr_{i,t}$ Squared voltage magnitude at node i at time t (kV^2).

$fl_{ij,t}$ Fictitious flow on branch (i, j) at time t.

$fg_{i,t}$ Fictitious supply at source node i at time t.

D. Binary Variables

$\alpha_{ij,t}$ Connection status of branch (i, j) at time t (1 if the branch is connected, 0 otherwise).

$c_{m,t}, d_{m,t}$ Charging and discharging status of MESS or EV fleet m at time t (1 if it is charging or discharging; 0 otherwise).

$\varphi_{m,t}$ Traveling status of MPS m at time t (1 if the MPS is traveling; 0 otherwise).

$\mu_{m,i,t}$ Connection status of MPS m to node i at time t (1 if connected; 0 otherwise).

I. Introduction

In the recent years, more frequent realization of the high-impact low-probability (HILP) natural disasters such as hurricanes, windstorms, earthquakes, etc. have resulted in prolonged electricity outages, excessive equipment damages, and even more severe economic loss and disruptions in our modern society [1], [2]. Earthquakes are the most unpredictable hazards which can cause striking damages in radial power distribution systems (DS). Among the past records on disastrous earthquakes, one can highlight the Loma Prieta earthquake in the greater San Francisco Bay Area in California in 1989 which caused $6 billion in property damage [3], the Northridge earthquake that struck Los Angeles on Jan 17, 1994, affecting 2.5 million local customers [4], Hanshin-Awaji region which was struck by the Hyogo-ken Nanbu earthquake on January 17, 1995, resulting approximately in 2.6 million households out of power services [5], the severe Bam earthquake in 2003 causing $90 million electricity reconstruction in Iran [6], the Wenchuan earthquake in 2008 which caused extreme damages in 966 substations, 274 transmission lines at multiple voltage levels and 1700 circuits damages [7], the Tohoku earthquake in 2011 impacting about 8.9 million households in 18 prefectures among 4 electric power companies [8], and recently in 2017 in Iran, the Sarpol-e Zahab earthquake with 7.3 moment magnitude resulting in a prolonged city-wide blackout for weeks [9].

As occurrence of such catastrophic HILP-caused electricity outages has been observed to be on the rise over the past decade [10], it calls for developing effective mechanisms that ensure a continuous and resilient supply of electricity to the end customers when dealing with the aftermath of seismic hazards. Power distribution system resilience to HILP events can be elevated by holistic planning, operation, and control of microgrids in which critical loads can be supplied during emergencies [11], [12]. Microgrids, as the physical islands (PI) in a local area, can be formed by utilizing distributed energy resources (DERs) to provide continuous power supply to electric utilities and customers [13]. Microgrids as an efficient mechanism to supply the critical loads during emergencies is studied in [14] where the restoration problem is transformed to a maximum coverage problem considering DERs' dynamic performance. The DERs, however, are typically deployed at fixed locations across the grid and thus are only able to support the local load points within a PI and maybe some in neighboring PIs, but certainly not the demanded loads in further-away PIs. Comparing with stationary microgrids with fixed-location DERs, mobile power sources (MPSs) which include mobile emergency generators (MEGs), electric vehicles (EVs), and truck-mounted mobile energy storage systems (MESSs) offer greater advantages as the grid-support resources to boost the DS resilience primarily driven by their mobility. The application of MPSs for enhanced resilience of DS has been studied in several research efforts [15]–[17]. Routing and scheduling of EVs is studied in [18] where EVs can be charged to store energy not only to meet its own transportation requirements, but also as an emergency power source to supply electricity to critical loads during emergencies [18]. Scheduling the charging and discharging of EVs is studied in [19] aiming to enhance the DS resilience against natural disasters. In [20], Vehicle-to-Home (V2H) technology, as a simplified variation of the vehicle-to-Grid (V2G) mechanism, is proposed as a backup power source to support the end customers during grid interruptions. MEG is studied in [13], [21] to recover the weather-caused outages and improve power system resilience. Following a HILP hazard, the configuration of the DS may change due to the unavailability of some distribution branches and other elements. DS network reconfiguration plays a significant role in rerouting and delivering the power from MPSs to critical loads by switching some branches on and off. The distribution branches can be equipped with remotely-controlled switches (RCS) that facilitate a network reconfiguration as emergency operating conditions unfold. Several models of DS network reconfiguration have been studies in the literature to improve the grid resilience in the face of emergencies [22]–[25].

978-1-5386-4539-0/19/$31.00 © 2019 IEEE

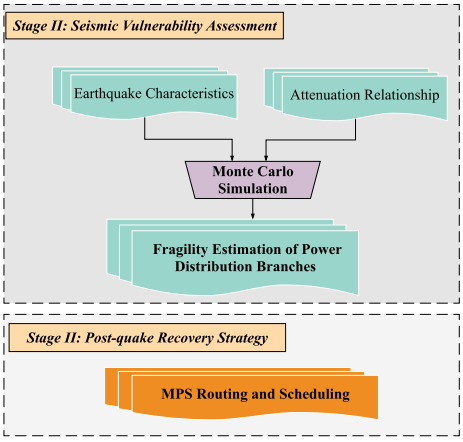

Fig. 1. Architecture of the proposed framework for earthquake resilience.

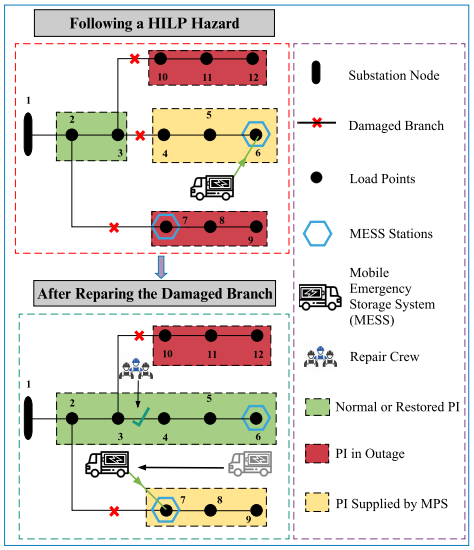

Fig. 2. Optimal routing and scheduling of MPSs following a seismic hazard.

In this paper, a suite of HILP seismic hazards is generated by Monte-Carlo simulation (MCS) engine which generates a huge set of earthquake scenarios to estimate the vulnerability of power distribution branches in the face of severe seismic forces. Then, a mixed-integer nonlinear programming (MINLP) model is proposed for routing and scheduling of MPSs coordinated with the DS network reconfiguration to improve the DS resilience against seismic hazards. The MINLP model is further linearized into a mixed-integer linear programming (MILP) model to decrease the computation complexity. Multiple types of MPSs, e.g., MEGs, MESSs and EVs, are dispatched considering the repair schedules of the damaged branches to facilitate the DS restoration process.

The rest of this paper is organized as follows. A big picture of the proposed model for MPSs dynamic dispatch and DS reconfiguration is presented in Section II. The proposed mix-integer linear programming formulation is presented in Section III. Numerical results and discussion are provided in Section IV. And Section V concludes the paper.

II. Big Picture: Proposed Architecture for DS Resilience to Seismic Hazards

A. Seismic Hazard Characterization and Overhead Lines' Vulnerability Assessment

The proposed architecture for power grid resilience against HILP earthquakes is demonstrated in Fig. 1. According to Fig. 1, the first step toward simulation of HILP seismic hazards is to generate a significant number of scenarios by MCS to estimate the peak ground acceleration (PGA) as a seismic intensity parameter at the location of power distribution branches. Fault mechanism, source specification, distance from the seismic source, the direction of seismic waves propagation, the properties of soil and sediments, and the geology and topology effects of the studied case are among factors which should be considered within an analytical attenuation relationship (AR) to properly model the attenuation of seismic waves energy. According to [26], a general formulation of the AR can be defined as follows:

$$\ln(\xi) = f(M) + f(R) + f(Z) + \epsilon \tag{1}$$

where ξ is the ground motion parameter, M is the earthquake magnitude, R is the distance between the source of earthquake and the studied case, and ϵ is a random error with mean value of zero and standard deviation of σ representing the uncertainty in ξ. Other parameters such as the site conditions, fault mechanism, sediment thickness, etc. can be mathematically modeled in a general form as $f(Z)$. Since power distribution branches do not have the same response to earthquake shocks, five damage states—*none*, *slight*, *moderate*, *extensive*, and *complete damage*—are introduced in this paper to assess the fragility of power distribution branches in the face of earthquakes [27]. According to [28], application of fragility curves is pursued in this paper by which the unavailability of power distribution line sections can be assessed. Each fragility curve is characterized by a median and log-normal standard deviation (σ), of the PGA parameter, which corresponds to the damage state thresholds and associated variability. The probability of residing in or exceeding a state of structural damage (γ) is described as follows:

$$P[\gamma|S_d] = \Phi[\frac{1}{\sigma_\gamma} \ln(\frac{S_d}{\overline{S}_{d,\gamma}})] \tag{2}$$

where, S_d is the spectral displacement; $\overline{S}_{d,\gamma}$ is its median value; σ_γ is the standard deviation corresponding to the natural logarithm of the spectral displacement at which a structure reaches the damage state threshold; and Φ is the standard cumulative normal distribution function.

B. Routing and Scheduling of MPS for Enhanced Resilience

Based on Fig. 2, the unavailability of some distribution branches following a seismic HILP event results in a number of physical islands (PIs) in which some or all load points are disconnected from the main grid. The optimal scheduling and routing of MPS can be achieved via the proposed optimization formulation with the aim of enhancing the DS resilience. Having identified the damaged branches in Stage I, the MPS can be moved to other PIs in which some portions of critical

978-1-5386-4539-0/19/$31.00 © 2019 IEEE

loads can be recovered by the excessive power provided by MPS. Meanwhile, the other damaged branches are repaired by repair crews and this loop is repeated until all damaged branches are repaired and all load points are supplied in the main grid. The system is then fully restored and the DS resilience function reaches its maximum.

III. Problem Formulation

This section presents an extensive formulation for routing and scheduling of MPS. Motivated by [19], the objective function (3) includes four terms, as follows:

$$\max(\sum_{t\in\mathbf{T}}\sum_{i\in\mathbf{B}}\chi_i\cdot pd_{i,t}-\sum_{t\in\mathbf{T}}\sum_{m\in\mathbf{M}}C_m^{\text{tr}}\cdot\varphi_{m,t}- \sum_{t\in\mathbf{T}}\sum_{m\in\{\mathbf{S},\mathbf{V}\}}|\frac{k_m}{100}|\cdot C_m^{\text{P}}\cdot(p_{m,t}^{\text{ch}}+p_{m,t}^{\text{dch}})-\sum_{t\in\mathbf{T}}\sum_{m\in\mathbf{G}}\delta_m\cdot p_{m,t}) \tag{3}$$

The first term is the total supplied load considering the priority of the load points over the entire time period; the second term is the transportation cost of MPSs due to the trips they make during the restoration phase; the third term reflects the cost of battery degradation when charging and discharging; and the last term is the relative cost of the MEG outputs. While there may exist various MPS dispatch strategies, the second term is added to minimize the traveling time of MPSs to avoid unnecessary transportation; the third term is aimed to reduce the battery degradation cost during the restoration phase; and the last term is added to minimize the cost associated with the output power of MEGs. A number of constraints need to be taken into account for the DS restoration problem as follows.

1) MPS Connection Constraints: Following a HILP disaster, the MPSs rapidly travel and get connected in the PIs to supply electricity where needed. At each time period, MPS can be connected to at most one pre-determined candidate node, as enforced in (4). Constraint (5) indicates that the allowed number of MPSs connected to a node is limited to stations' capacity at each candidate node. Constraint (6) states that the MPSs cannot travel to other nodes when connected to a candidate node.

$$\sum_{i\in\mathbf{B}_m}\mu_{m,i,t}\le 1,\forall m\in\mathbf{M},\forall t\in\mathbf{T} \tag{4}$$

$$\sum_{m\in\mathbf{M}_i}\mu_{m,i,t}\le N_i^{\text{mps}},\forall i\in\bigcup_{m\in\mathbf{M}}\mathbf{B}_m,\forall t\in\mathbf{T} \tag{5}$$

$$\varphi_{m,t}=1-\sum_{i\in\mathbf{B}_m}\mu_{m,i,t},\forall m\in\mathbf{M},\forall t\in\mathbf{T} \tag{6}$$

2) MPS Routing Constraints: constraint (7) ensures that the MPSs transportation among different DS nodes satisfies the required travel time.

$$\mu_{m,i,t+\tau}+\mu_{m,j,t}\le 1,\ \forall m\in\mathbf{M},\ \forall i,j\in\mathbf{B}_m,\ \forall\tau\le T_{m,ij}^{\text{travel}},\ \forall t+\tau\le N_{\mathbf{T}} \tag{7}$$

3) MPS Power Scheduling Constraints: It is assumed that the trunk-mounted MESS and MEG can be refueled with tanker trunk for transportation during the restoration process [29], while EVs consume electric energy when they are in transport. The change in the state of charge (SOC) of MESSs over time is determined by their charging and discharging behaviors, as represented in (8) while the SOC of EVs is determined by their charging and discharging as well as travel behaviors (9). Constraint (10) restricts the range of SOC of MESS and EV over all time periods. Constraint (11) and (12) respectively impose the range of charging and discharging power for MESS and EV according to the corresponding rated power. The charging and discharging power are both enforced to be zero when MESS and EV are not connected to the DS. Charging and discharging of MESS and EV are mutually exclusive over all time periods, as represented in (13) which indicates that the MPS disconnected from DS can neither charge nor discharge. Constraint (14) and (15) set the range of real and reactive power output of MEG according to its rated power, respectively, and enforce MEG to have zero real and reactive output when it is disconnected from DS.

$$\text{SOC}_{m,t}=\text{SOC}_{m,t-1}+(\eta_m^{\text{ch}}\cdot p_{m,t}^{\text{ch}}-p_{m,t}^{\text{dch}}/\eta_m^{\text{dch}})\cdot\Delta t,\quad\forall m\in\mathbf{S},\ \forall t\ge 1 \tag{8}$$

$$\text{SOC}_{m,t}=\text{SOC}_{m,t-1}+(\eta_m^{\text{ch}}\cdot p_{m,t}^{\text{ch}}-p_{m,t}^{\text{dch}}/\eta_m^{\text{dch}}-\varphi_{m,t}\cdot P_m^{\text{travel}})\cdot\Delta t,\quad\forall m\in\mathbf{V},\ \forall t\ge 1 \tag{9}$$

$$\underline{\text{SOC}}_m\le\text{SOC}_{m,t}\le\overline{\text{SOC}}_m,\forall m\in\{\mathbf{S},\mathbf{V}\},\forall t\in\mathbf{T} \tag{10}$$

$$0\le p_{m,t}^{\text{ch}}\le c_{m,t}\cdot\overline{P}_m^{\text{ch}},\forall m\in\{\mathbf{S},\mathbf{V}\},\forall t\in\mathbf{T} \tag{11}$$

$$0\le p_{m,t}^{\text{dch}}\le d_{m,t}\cdot\overline{P}_m^{\text{dch}},\forall m\in\{\mathbf{S},\mathbf{V}\},\forall t\in\mathbf{T} \tag{12}$$

$$c_{m,t}+d_{m,t}\le\sum_{i\in\mathbf{B}_m}\mu_{m,i,t},\forall m\in\{\mathbf{S},\mathbf{V}\},\forall t\in\mathbf{T} \tag{13}$$

$$0\le p_{m,t}\le\sum_{i\in\mathbf{B}_m}\mu_{m,i,t}\cdot\overline{P}_m,\forall m\in\mathbf{G},\forall t\in\mathbf{T} \tag{14}$$

$$0\le q_{m,t}\le\sum_{i\in\mathbf{B}_m}\mu_{m,i,t}\cdot\overline{Q}_m,\forall m\in\mathbf{G},\forall t\in\mathbf{T} \tag{15}$$

4) DS Radiality Constraints: Constraints (16)-(19) ensure that the DS remains radial over all time periods. For DS radiality, there are two conditions which need to be satisfied: (i) at each PI, the number of connected branches is equal to the total number of nodes in the PI - 1; (ii) all load points are connected to a determined source node in each PI. The first condition is satisfied in constraint (16). In each PI, one node is considered as a fictitious source node and the remaining nodes are fictitious load points. The fictitious source node and fictitious load node are the source and the destination of fictitious power flow, respectively. The amount of the fictitious flow into a load node $d_{i,t}^{\text{fic}}$ is set as 1 at all nodes. The second condition is satisfied in constraint (17)-(19) that enforce each load node to receive one unit of the fictitious flow from the fictitious source node at each PI. Constraints (17)-(18) ensure the fictitious flow balance for the fictitious load and source nodes, respectively. Constraint (19) enforces the fictitious flow to be zero in open branches. The large enough positive number M relaxes this constraint when some branches are open (See [30] for additional details on the fictitious network and radiality conditions).

$$\sum_{(i,j)\in\mathbf{L}}\alpha_{ij,t}=N_{\mathbf{B}}-N_t^{\text{island}},\forall t\in\mathbf{T} \tag{16}$$

978-1-5386-4539-0/19/$31.00 © 2019 IEEE

$$\sum_{(j,i)\in\mathbf{L}} fl_{ji,t} - \sum_{(i,j)\in\mathbf{L}} fl_{ij,t} = d_{i,t}^{\text{fic}}, \forall i \in \mathbf{B}\backslash\mathbf{B}_t^{\text{source}}, \forall t \in \mathbf{T} \tag{17}$$

$$\sum_{(i,j)\in\mathbf{L}} fl_{ij,t} - \sum_{(j,i)\in\mathbf{L}} fl_{ji,t} = fg_{i,t}, \forall i \in \mathbf{B}_t^{\text{source}}, \forall t \in \mathbf{T} \tag{18}$$

$$-\alpha_{ij,t}\cdot M \le fl_{ij,t} \le \alpha_{ij,t}\cdot M, \forall (i,j)\in\mathbf{L}, \forall t\in\mathbf{T} \tag{19}$$

5) Branch Status Constraints: According to (20), the damaged branch must be open if it has not yet been repaired at time t. Constraint (21) states that the undamaged branches without RCS remain in their initial status over all time periods.

$$\alpha_{ij,t} \le \beta_{ij,t}, \forall (i,j)\in\mathbf{L}, \forall t\in\mathbf{T} \tag{20}$$

$$\alpha_{ij,t} = \alpha_{ij}^0, \forall (i,j)\in\mathbf{L}\backslash\{\mathbf{L}_t^{\text{damaged}}, \mathbf{L}^{\text{switch}}\}, \forall t\in\mathbf{T} \tag{21}$$

6) MPS Output Power Constraints: Constraints (22)-(23) indicate that the real or reactive power injection or extraction at a candidate node for MPS siting is equal to the sum of the real or reactive power output of the MPSs. The non-MPS nodes are attributed zero real and reactive power from MPSs as expressed in (24).

$$p_{i,t}^{\text{mps}} = \sum_{m\in\mathbf{M}_i\cap\{\mathbf{S},\mathbf{V}\}} \mu_{m,i,t}\cdot p_{m,t}^{\text{dch}} - \sum_{m\in\mathbf{M}_i\cap\{\mathbf{S},\mathbf{V}\}} \mu_{m,i,t}\cdot p_{m,t}^{\text{ch}} + \sum_{m\in\mathbf{M}_i\cap\mathbf{G}} \mu_{m,i,t}\cdot p_{m,t}, \quad \forall i \in \bigcup_{m\in\mathbf{M}} \mathbf{B}_m, \forall t\in\mathbf{T} \tag{22}$$

$$q_{i,t}^{\text{mps}} = \sum_{m\in\mathbf{M}_i} \mu_{m,i,t}\cdot q_{m,t}, \quad \forall i \in \bigcup_{m\in\mathbf{M}} \mathbf{B}_m, \forall t\in\mathbf{T} \tag{23}$$

$$p_{i,t}^{\text{mps}} = q_{i,t}^{\text{mps}} = 0, \quad \forall i \in \mathbf{B}\backslash \bigcup_{m\in\mathbf{M}} \mathbf{B}_m, \forall t\in\mathbf{T} \tag{24}$$

7) Power Balance Constraints: Constraints (25)-(26) describe the real and reactive power balance conditions at all nodes, respectively. The range of the demanded load to be supplied is bounded in constraint (27). Constraint (28) enforces the recovery rate of the supplied loads not to decrease. The power factor of the demand is assumed to be fixed in (29). The real and reactive power flows in the online branches are respectively limited by their real and reactive power capacities in (30)-(31). Constraints (30)-(31) also enforce the real and reactive power flow in open branches to be zero.

$$\sum_{(j,i)\in\mathbf{L}} pf_{ji,t} - \sum_{(i,j)\in\mathbf{L}} pf_{ij,t} = pd_{i,t} - pg_{i,t} - p_{i,t}^{\text{mps}}, \quad \forall i\in\mathbf{B}, \forall t\in\mathbf{T} \tag{25}$$

$$\sum_{(j,i)\in\mathbf{L}} qf_{ji,t} - \sum_{(i,j)\in\mathbf{L}} qf_{ij,t} = qd_{i,t} - qg_{i,t} - q_{i,t}^{\text{mps}}, \quad \forall i\in\mathbf{B}, \forall t\in\mathbf{T} \tag{26}$$

$$0 \le pd_{i,t} \le P_{i,t}^{\text{demand}}, \forall i\in\mathbf{B},\ \forall t\in\mathbf{T} \tag{27}$$

$$pd_{i,t-1}/P_{i,t-1}^{\text{demand}} \le pd_{i,t}/P_{i,t}^{\text{demand}}, \forall i\in\mathbf{B},\ \forall t\ge 1 \tag{28}$$

$$qd_{i,t} = (Q_{i,t}^{\text{demand}}/P_{i,t}^{\text{demand}})\cdot pd_{i,t}, \forall i\in\mathbf{B},\ \forall t\in\mathbf{T} \tag{29}$$

$$-\alpha_{ij,t}\cdot\overline{P}_{ij} \le pf_{ij,t} \le \alpha_{ij,t}\cdot\overline{P}_{ij}, \forall (i,j)\in\mathbf{L}, \forall t\in\mathbf{T} \tag{30}$$

$$-\alpha_{ij,t}\cdot\overline{Q}_{ij} \le qf_{ij,t} \le \alpha_{ij,t}\cdot\overline{Q}_{ij}, \forall (i,j)\in\mathbf{L}, \forall t\in\mathbf{T} \tag{31}$$

8) Power Flow Constraints: Constraint (32) and (33) represent the power flow equation in which the M value is a relaxation parameter [31]. Constraint (34) states the boundary for the voltage magnitudes.

$$Vsqr_{i,t} - Vsqr_{j,t} \le (1-\alpha_{ij,t})\cdot M + 2\cdot(r_{ij}\cdot pf_{ij,t} + x_{ij}\cdot qf_{ij,t}), \quad \forall (i,j)\in\mathbf{L}, \forall t\in\mathbf{T} \tag{32}$$

$$Vsqr_{i,t} - Vsqr_{j,t} \ge (\alpha_{ij,t}-1)\cdot M + 2\cdot(r_{ij}\cdot pf_{ij,t} + x_{ij}\cdot qf_{ij,t}), \quad \forall (i,j)\in\mathbf{L}, \forall t\in\mathbf{T} \tag{33}$$

$$\underline{\text{Vsqr}}_i \le Vsqr_{i,t} \le \overline{\text{Vsqr}}_i, \forall i\in\mathbf{B}, \forall t\in\mathbf{T} \tag{34}$$

Note that constraints (22) and (23) include non-linear terms making the optimization problem a mixed-integer non-linear programming (MINLP) model. we propose a linearization technique as illustrated below [32]:

$$0 \le P_{m,i,t}^{\text{dch}} \le \mu_{m,i,t}\cdot\overline{P}_m^{\text{dch}} \tag{35}$$

$$p_{m,t}^{\text{dch}} + (\mu_{m,i,t}-1)\cdot\overline{P}_m^{\text{dch}} \le P_{m,i,t}^{\text{dch}} \le p_{m,t}^{\text{dch}} \tag{36}$$

where, if $\mu_{m,i,t} = 1$, then we have $P_{m,i,t}^{\text{dch}} = p_{m,t}^{\text{dch}}$; if $\mu_{m,i,t} = 0$, then $P_{m,i,t}^{\text{dch}} = 0$. By doing so, the MINLP formulation is linearized into a mixed-integer linear programming (MILP) problem and, therefore, the computation complexity is significantly reduced.

IV. Numerical Results and Discussions

In order to verify the effectiveness of the proposed scheme for DS seismic resilience, the IEEE 33-node test system is employed as the testbed. All simulations have been conducted on a PC with an Intel Xeon E5-2620 v2 processor and 16 GB of memory using CPLEX 12.5.1.

We generated 100,000 earthquake scenarios via the MCS, where it was identified that 9 branches out of the 37 branches in the network have a remarkable fragility comparatively. The set of damaged branches in the network, L^{damaged}, in the face of the generated earthquake scenarios are illustrated in Fig. 3 at time slot $t = 1 \sim 2$. The allocation of 8 RCS is also demonstrated in Fig.3 [33]. The total time period is considered $T = 24$, where each time period is Δt=0.5h. It is assumed that 3 MESS stations are available in the DS network to connect the MEG and MESS [34] and there are 3 charging stations for EVs [35] [36]. All the MPSs are located at the substation node at $t = 1$ and the initial SOC of EV and MESS are considered fully charged. Moreover, we assume that 3 MPSs are available in the restoration process: one EV, one MESS and one MEG. The repair schedule for damaged branches is assumed as follows: branch 19-20 at *t*=3, branch 8-9 at *t*=6, branch 9-10 at *t*=7, branch 12-13 at *t*=9, branch 16-17 at *t*=13, branch 30-31 at *t*=16, branch 27-28 at *t*=20, branch 24-25 at *t*=22, branch 23-24 at *t*=24 will be repaired.

The restoration process is demonstrated in Fig. 3, where only some restoration time periods are presented due to the space limitations in this manuscript. The location of MPSs at each time period during the restoration phase is illustrated in Fig. 4 in which the symbol "→" denotes that the MPS

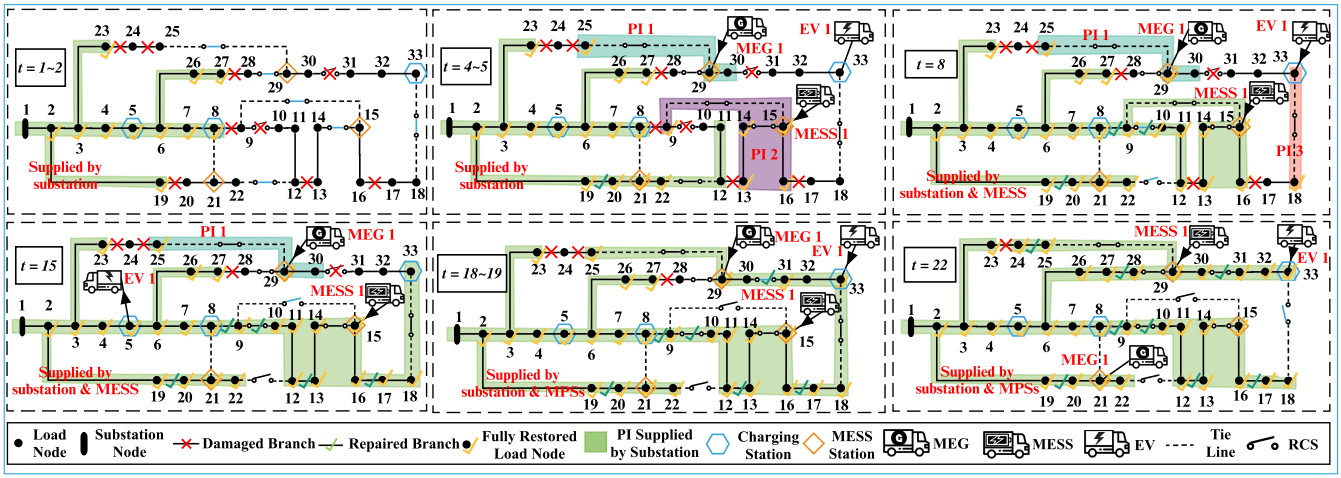

Fig. 3. Restoration process coordinated with MPSs dispatch and DS dynamic reconfiguration.

is travelling between different nodes. The power profile of the MPSs at each time period during the restoration process is illustrated in Fig. 5. Following an adverse seismic event, at t=1∼2, tie lines 9-15, 12-22, 18-33, and 25-29 which are normally open (i.e., offline) should be closed (i.e., online) in order to change the DS topology such several PIs can be linked to facilitate the MPSs contribution in recovery of load outages in the subsequent time periods. Note that branch 14-15 and 28-29 are already online during the normal operating conditions, while branches 9-10 and 30-31 are offline due to post-quake damages. Besides, all MPSs should be departed from the substation node at time t=1. At t=4∼5, branch 19-20 has been repaired by repair crews; MEG 1 and MESS 1 are connected to node 29 and 15, respectively, to form PI 1 and PI 2. While EV 1 reaches the node 33, it should not be discharged since the energy is reserved for the subsequent recovery time periods. According to Fig. 5, at t=7, EV 1 starts supplying power in PI 3. Meanwhile, branch 12-22 is open to ensure the DS radial topology since branches 8-9 and 9-10 are repaired and connected back at t=6 and t=7, respectively. At t=8, the load points in PI 2 can be supplied by the main grid as well as the extra power provided by MESS 1. At t=9, branch 9-15 is open to ensure the DS radial topology since branch 12-13 is repaired and connected back. At t=15, the branch 16-17 has been repaired; hence, nodes 17, 18, and 33 are re-connected to the substation node and PI 3 is merged with the main grid. EV 1 should travel to node 5 in order to be charged since its SOC is reaching the minimum threshold. At t=18∼19, branch 30-31 has been repaired when EV 1 returns to node 33 and continues supplying the neighbour load points as they have not been yet fully restored—due to the distribution lines capacity limits. Moreover, all load points across the studied DS, except node 24, are supplied with the energy conjointly provided by the main grid and the MPSs at t=18∼19. At t=20, branch 27-28 is repaired and re-energized; therefore, branch 18-33 is open to ensure the DS radial topology. At t=22, branch 24-25 is repaired, the DS is fully restored by the main grid substation and all the grid-support MPS resources even though branch 23-24 is not yet repaired.

In summary, the proposed model for utilizing the MPSs

---		Time Period								
		1	2~3	4~12	13~14	15	16~17	18~19	20	21	22~24
MPS	EV 1	node 1	→	node 33	→	node 5	→	node 33			
	MESS 1	node 1	→	node 15					→	node 29	
	MEG 1	node 1	→	node 29					→	node 21	

Fig. 4. Location of MPSs at each time period during the restoration process.

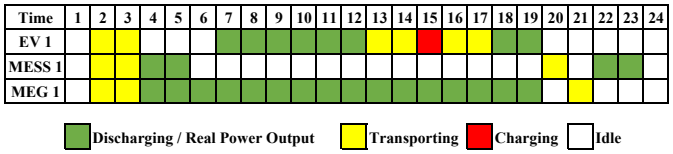

Fig. 5. MPSs power profile in each time period during the restoration process.

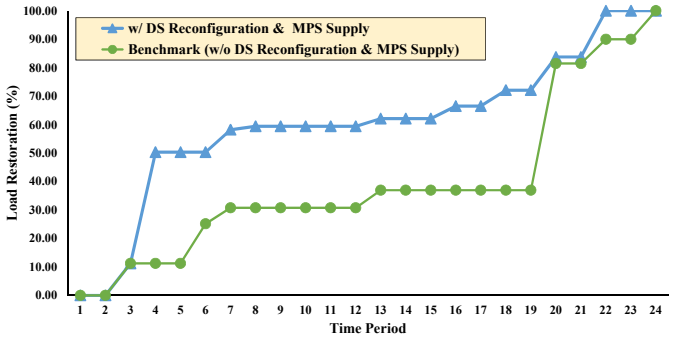

Fig. 6. Load restoration in each time period in different studied test cases.

conjointly with harnessing the built-in flexibility of the DS topology (through DS dynamic reconfiguration) has resulted in 100% load outage recovery at t=22, as illustrated in Fig. 6. It should be noted that at t=3∼19, the recovery rate of the proposed model is 40% higher than the base-case where neither DS network reconfiguration nor MPS supply is employed. This further highlights the role of the MPSs in DS restoration if well planned, scheduled, and coordinated with other flexible resources. The numerical results verified that the proposed model can not only effectively reduce the amount of load outages, but also ensures a swift response and recovery, thereby realizing an enhanced operational resilience to HILP earthquakes.

V. Conclusion

This paper proposes a co-optimization approach to improve the DS operational resilience in dealing with the aftermath of HILP seismic hazards. Seismic hazard characterization is accomplished by a suite of simulated earthquake scenarios via a Monte-Carlo simulation engine to evaluate the fragility (vulnerability) of the distribution branches in the face of seismic forces. A MINLP optimization model is suggested, linearized, and reformulated to a MILP model in order to achieve an effective restoration strategy that unlocks the full potential of MPSs (effective routing and scheduling) and the dynamic DS network reconfiguration (effective utilization of the grid built-in flexibility using the existing infrastructure), all in coordination with the repair crew schedules. Numerical results demonstrated that the proposed approach could effectively facilitate the DS restoration through a swift response and recovery, resulting in a significant reduction in the outage extent and duration, thereby realizing an enhanced operational resilience to HILP earthquakes.

References

[1] B. Zhang, P. Dehghanian, and M. Kezunovic, "Optimal allocation of pv generation and battery storage for enhanced resilience," *IEEE Transactions on Smart Grid*, vol. 10, no. 1, pp. 535–545, 2017.

[2] P. Dehghanian, S. Aslan, and P. Dehghanian, "Maintaining electric system safety through an enhanced network resilience," *IEEE Transactions on Industry Applications*, vol. 54, no. 5, pp. 4927–4937, 2018.

[3] Major California earthquakes, [Online] Available: https://cnico.com/pgs/earthquake/earth3.aspx.

[4] R. J. Campbell, "Weather-related power outages and electric system resiliency," Congressional Research Service, Library of Congress Washington, DC, 2012.

[5] Y. Kitagawa and H. Hiraishi, "Overview of the 1995 hyogo-ken nanbu earthquake and proposals for earthquake mitigation measures," *Journal of Japan association for earthquake engineering*, vol. 4, no. 3, pp. 1–29, 2004.

[6] M. Ghafory-Ashtiany and M. Hosseini, "Post-bam earthquake: recovery and reconstruction," *Natural Hazards*, vol. 44, no. 2, pp. 229–241, 2008.

[7] J. Eidinger, "Wenchuan earthquake impact to power systems," in *TCLEE 2009: Lifeline Earthquake Engineering in a Multihazard Environment*, pp. 1–12, 2009.

[8] Y. Kuwata and Y. Ohnishi, "Emergency-response capacity of lifelines after wide-area earthquake disasters," in *Proc. Int. Symp. Eng. Lessons Learned Great East Jpn. Earthquake*, pp. 1475–1486, 2011.

[9] M. Zare, F. Kamranzad, I. Parcharidis, and V. Tsironi, "Preliminary report of mw7. 3 sarpol-e zahab, iran earthquake on november 12, 2017," *Tehran, Iran: International Institute of Earthquake Engineering and Seismology (IIEES)*, 2017.

[10] P. Dehghanian, B. Zhang, T. Dokic, and M. Kezunovic, "Predictive risk analytics for weather-resilient operation of electric power systems," *IEEE Transactions on Sustainable Energy*, vol. 10, no. 1, pp. 3–15, 2019.

[11] K. P. Schneider, F. K. Tuffner, M. A. Elizondo, C.-C. Liu, Y. Xu, and D. Ton, "Evaluating the feasibility to use microgrids as a resiliency resource," *IEEE Transactions on Smart Grid*, vol. 8, no. 2, pp. 687–696, 2017.

[12] J. Lai, X. Lu, F. Wang, P. Dehghanian, and R. Tang, "Broadcast gossip algorithms for distributed peer-to-peer control in ac microgrids," *IEEE Transactions on Industry Applications*, 2019.

[13] P. M. de Quevedo, J. Contreras, A. Mazza, G. Chicco, and R. Porumb, "Reliability assessment of microgrids with local and mobile generation, time-dependent profiles, and intraday reconfiguration," *IEEE Transactions on Industry Applications*, vol. 54, no. 1, pp. 61–72, 2018.

[14] Y. Xu, C.-C. Liu, K. P. Schneider, F. K. Tuffner, and D. T. Ton, "Microgrids for service restoration to critical load in a resilient distribution system," *IEEE Transactions on Smart Grid*, vol. 9, no. 1, pp. 426–437, 2018.

[15] J. Kim and Y. Dvorkin, "Enhancing distribution system resilience with mobile energy storage and microgrids," *IEEE Transactions on Smart Grid*, 2018.

[16] S. Lei, C. Chen, Y. Li, and Y. Hou, "Resilient disaster recovery logistics of distribution systems: Co-optimize service restoration with repair crew and mobile power source dispatch," *IEEE Transactions on Smart Grid*, 2019.

[17] B. Wang, J. A. Camacho, G. M. Pulliam, A. H. Etemadi, and P. Dehghanian, "New reward and penalty scheme for electric distribution utilities employing load-based reliability indices," *IET Generation, Transmission & Distribution*, vol. 12, no. 15, pp. 3647–3654, 2018.

[18] Y. Ma, T. Houghton, A. Cruden, and D. Infield, "Modeling the benefits of vehicle-to-grid technology to a power system," *IEEE Transactions on power systems*, vol. 27, no. 2, pp. 1012–1020, 2012.

[19] S. Lei, C. Chen, H. Zhou, and Y. Hou, "Routing and scheduling of mobile power sources for distribution system resilience enhancement," *IEEE Transactions on Smart Grid*, 2018.

[20] H. Shin and R. Baldick, "Plug-in electric vehicle to home (v2h) operation under a grid outage," *IEEE Transactions on Smart Grid*, vol. 8, no. 4, pp. 2032–2041, 2017.

[21] S. Lei, J. Wang, C. Chen, and Y. Hou, "Mobile emergency generator pre-positioning and real-time allocation for resilient response to natural disasters," *IEEE Transactions on Smart Grid*, vol. 9, no. 3, pp. 2030–2041, 2018.

[22] J. A. Taylor and F. S. Hover, "Convex models of distribution system reconfiguration," *IEEE Transactions on Power Systems*, vol. 27, no. 3, pp. 1407–1413, 2012.

[23] T. E. McDermott, I. Drezga, and R. P. Broadwater, "A heuristic nonlinear constructive method for distribution system reconfiguration," *IEEE Transactions on Power Systems*, vol. 14, no. 2, pp. 478–483, 1999.

[24] Y.-K. Wu, C.-Y. Lee, L.-C. Liu, and S.-H. Tsai, "Study of reconfiguration for the distribution system with distributed generators," *IEEE transactions on Power Delivery*, vol. 25, no. 3, pp. 1678–1685, 2010.

[25] R. S. Rao, K. Ravindra, K. Satish, and S. Narasimham, "Power loss minimization in distribution system using network reconfiguration in the presence of distributed generation," *IEEE transactions on power systems*, vol. 28, no. 1, pp. 317–325, 2013.

[26] O. W. Nuttli, "Seismic wave attenuation and magnitude relations for eastern north america," *Journal of Geophysical Research*, vol. 78, no. 5, pp. 876–885, 1973.

[27] C. A. Kircher, R. V. Whitman, and W. T. Holmes, "Hazus earthquake loss estimation methods," *Natural Hazards Review*, vol. 7, no. 2, pp. 45–59, 2006.

[28] H. FEMA, "Multi-hazard loss estimation methodology, earthquake model," *Washington, DC, USA: Federal Emergency Management Agency*, 2003.

[29] S. Iwai, T. Kono, M. Hashiwaki, and Y. Kawagoe, "Use of mobile engine generators as source of back-up power," in *INTELEC 2009-31st International Telecommunications Energy Conference*, pp. 1–6, IEEE, 2009.

[30] M. Lavorato, J. F. Franco, M. J. Rider, and R. Romero, "Imposing radiality constraints in distribution system optimization problems," *IEEE Transactions on Power Systems*, vol. 27, no. 1, pp. 172–180, 2012.

[31] M. E. Baran and F. F. Wu, "Network reconfiguration in distribution systems for loss reduction and load balancing," *IEEE Transactions on Power delivery*, vol. 4, no. 2, pp. 1401–1407, 1989.

[32] W. Wei, F. Liu, S. Mei, and Y. Hou, "Robust energy and reserve dispatch under variable renewable generation," *IEEE Transactions on Smart Grid*, vol. 6, no. 1, pp. 369–380, 2015.

[33] S. Lei, J. Wang, and Y. Hou, "Remote-controlled switch allocation enabling prompt restoration of distribution systems," *IEEE Transactions on Power Systems*, vol. 33, no. 3, pp. 3129–3142, 2018.

[34] H. H. Abdeltawab and Y. A.-R. I. Mohamed, "Mobile energy storage scheduling and operation in active distribution systems," *IEEE Transactions on Industrial Electronics*, vol. 64, no. 9, pp. 6828–6840, 2017.

[35] X. Yan, C. Duan, X. Chen, and Z. Duan, "Planning of electric vehicle charging station based on hierarchic genetic algorithm," in *2014 IEEE Conference and Expo Transportation Electrification Asia-Pacific (ITEC Asia-Pacific)*, pp. 1–5, IEEE, 2014.

[36] A. Briones, J. Francfort, P. Heitmann, M. Schey, S. Schey, and J. Smart, "Vehicle-to-grid (v2g) power flow regulations and building codes review by the avta," *Idaho National Lab., Idaho Falls, ID, USA*, 2012.